Journal of Inorganic Biochemistry 279 (2026) 113272

Contents lists available at ScienceDirect

Journal of Inorganic Biochemistry

journal homepage: www.elsevier.com/locate/jinorgbio

Structure-activity studies reveal efficient inactivation of urease by Ebsulfur-based compounds

Luca Mazzei [a,*], Arundhati Paul [a], Michele Cianci [b], Andrea Pizzi [c], Giuseppe Resnati [c], Stefano Ciurli [a]

[a] Laboratory of Bioinorganic Chemistry, Department of Pharmacy and Biotechnology (FaBiT), University of Bologna, I-40138 Bologna, Italy
[b] Department of Agricultural, Food and Environmental Sciences, Polytechnic University of Marche, I-60131 Ancona, Italy
[c] Department of Chemistry, Materials, and Chemical Engineering "Giulio Natta", Politecnico di Milano, I-20131 Milano, Italy

ARTICLE INFO

Keywords:
Urease
Nickel
Sulfur
X-ray crystallography
Enzyme kinetics
Inhibition

ABSTRACT

Antimicrobial resistance is one of the most significant global health threats of the 21st century, demanding urgent strategies for the development of novel therapeutic approaches. Urease, a nickel-dependent enzyme absent in the human proteome, represents an attractive target for drug development because several urease-expressing bacterial pathogens play a critical role in pathogenesis. Alternative strategies, such as drug repurposing, are necessary to uncover the potential of antimicrobial molecules. In this context, the organo-selenium compound Ebselen has shown promising urease-inhibitory properties, but its therapeutic application is limited by toxicity concerns. Ebsulfur, a sulfur analog of Ebselen, offers a potentially safer alternative. In this study, we evaluated three Ebsulfur derivatives for their ability to inhibit urease from *Sporosarcina pasteurii* and *Canavalia ensiformis*. Biochemical assays demonstrated that these compounds effectively inactivate both bacterial and plant urease in the low micromolar range. The X-ray crystal structures of *Sporosarcina pasteurii* urease co-crystallized with two of the derivatives, determined at 1.95–1.96 Å resolution, suggested a mechanism involving di-sulfuration of the catalytically essential αCys322 residue. These findings provide insight into the potential of Ebsulfur derivatives as antimicrobial agents, addressing the persistent lack of progress in antibiotic development, and contribute to the development of alternative antimicrobial strategies targeting resistant pathogens.

1. Introduction

Antimicrobial resistance has emerged among the top ten public health threats of the 21st century, causing millions of deaths and tremendous socioeconomic costs [1,2]. Each year, around 7.7 million deaths are estimated to be caused by bacterial infections, of which 4.9 million are associated with drug-resistant pathogens, and 1.3 million are directly ascribable to bacterial pathogens resistant to the antibiotics available [3]. The World Health Organization has published and updated, since 2017, a Bacterial Priority Pathogens List (BPPL) with the aim of guiding research, development, and strategies to prevent and control antimicrobial resistance by bacterial pathogens of public health importance [4]. The 2024 BPPL update [5] includes several bacterial species, such as *Klebsiella pneumoniae*, *Mycobacterium tuberculosis*, *Pseudomonas aeruginosa*, *Staphylococcus aureus*, *Proteus mirabilis*, and *Haemophilus influenzae*, which express the virulence factor urease, a nickel-dependent enzyme able to hydrolyze urea to give carbon dioxide and ammonia [6–13]. The pathogenesis of these bacteria is strongly related to their ureolytic activity, which causes the increase in pH and the toxicity of ammonia accumulated in the microbial microenvironment and the host [14,15]. Outside this set of microorganisms, but nevertheless a paradigmatic ureolytic bacterium acting as human pathogen, is *Helicobacter pylori*, which colonizes the acidic stomach environment inducing gastric inflammation and increasing the risk of developing duodenal and gastric ulcers, adenocarcinoma, and lymphoma [11,16,17].

The key role that urease plays as a virulence factor, and its absence in the human genome, renders this enzyme an attractive target for drug discovery efforts against diseases caused by antimicrobial-resistant pathogens. However, this potential is hindered by the persistent lack of breakthroughs in antimicrobials discoveries over recent decades, which continues to limit the development of effective therapies to

* Corresponding author.
E-mail addresses: luca.mazzei2@unibo.it (L. Mazzei), arundhati.paul2@unibo.it (A. Paul), m.cianci@staff.univpm.it (M. Cianci), andrea.pizzi@polimi.it (A. Pizzi), giuseppe.resnati@polimi.it (G. Resnati), stefano.ciurli@unibo.it (S. Ciurli).

https://doi.org/10.1016/j.jinorgbio.2026.113272
Received 24 September 2025; Received in revised form 4 December 2025; Accepted 18 February 2026
Available online 21 February 2026

combat the global threat of antimicrobial resistance [18,19]. This challenge can be addressed through drug repurposing initiatives [20], namely by identifying new molecular targets and novel uses for existing drugs. Such approaches bypass the complexity of conventional drug discovery pipelines, offering more efficient and cost-effective opportunities for drug development.

In this context, the organo-selenium compound Ebselen (2-phenyl-1,2-benzisoselenazol-3(2H)-one) has recently emerged as a promising candidate for drug repurposing (Scheme 1). Ebselen exhibits antimicrobial activity against various Gram-positive and Gram-negative bacterial strains [21,22] and has undergone numerous clinical trials for the potential treatment of a wide range of diseases. Beyond its well-known redox activity as a glutathione peroxidase (GPx) mimic, Ebselen has been investigated for treating acute ischemic stroke, diabetes mellitus, Ménière's disease, and acute noise-induced hearing loss, among others [23]. This broad therapeutic potential suggests that Ebselen interacts with multiple molecular targets, particularly thiol-containing proteins. Supporting this hypothesis, Ebselen has been shown to inactivate ureases from different sources [24–26] through the covalent modification of a conserved and essential cysteine residue, as revealed by the X-ray crystal structure of *Sporosarcina pasteurii* urease (SPU) treated with an Ebselen derivative [25]. In particular, the thiol group of αCys322 (SPU numbering) undergoes a di-selenation reaction, a process proposed to be mediated by an adjacent and conserved histidine residue (αHis323) [25]. The αCys322-αHis323 catalytic dyad is located at the tip of a helix-turn-helix motif (mobile flap) that is crucial for urease activity. This motif can be found in an *open* or *closed* conformation: in the *open* state it facilitates the transit of substrate and products through the active-site channel connecting the bulk solvent with the catalytic cavity, while in its *closed* state it regulates the positioning of essential amino acid residues within the active site during catalysis, among which the αCys322 - αHis323 catalytic dyad is involved in the proton transfer to the reaction intermediate (Fig. 1). The covalent adduct formed upon Ebselen treatment inhibits enzyme activity by preventing a correct closure of the flap during catalysis and the participation of the αCys322-αHis323 dyad in the catalytic mechanism [25].

The thiol-oxidizing properties of Ebselen and its derivatives are considered the primary molecular basis of the chronic toxicity of Ebselen and, more broadly, of organo-selenium compounds [28]. Extensive literature reports indicate that Ebselen potential as a therapeutic drug may be limited by its toxic effects [28–32], which include mitochondrial dysfunction [33–35], genotoxicity and DNA damage [36,37], alterations in DNA-binding mechanisms of cysteine- and zinc-containing transcription factors [38], and the induction of apoptosis [39]. Selenium in fact exhibits a dual effect depending on its concentration, a phenomenon known as the 'selenium paradox' [40]. At low concentrations (below 0.1 μM), selenium deficiency is associated with various health issues, including cardiomyopathy and increased susceptibility to viral infections. Within an optimal range (approximately 1 μM), selenium acts as an antioxidant by promoting the expression of seleno-proteins that

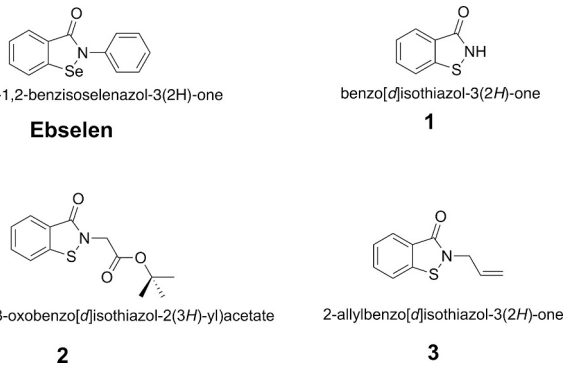

Scheme 1.

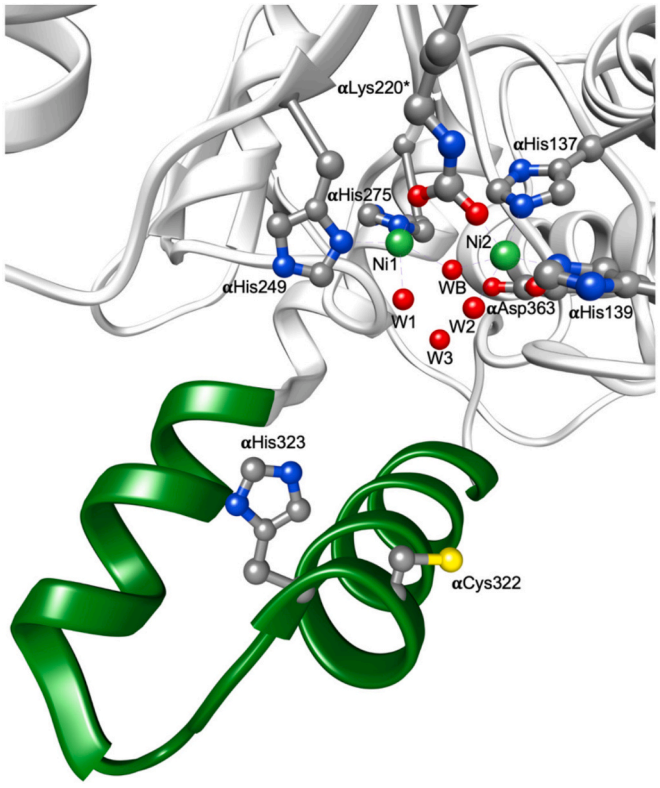

Fig. 1. Active site of SPU showing the coordination environment of the Ni(II) ions and the location of the mobile flap (shown in green) in front of the active site pocket. The figure was generated using UCSF Chimera [27]. (For interpretation of the references to colour in this figure legend, the reader is referred to the web version of this article.)

regulate reactive oxygen species (ROS) [41]. However, at higher concentrations (1–10 μM), selenium can have pro-oxidant effects, a feature that has been explored for potential anticancer applications [42,43].

Ebsulfur, the sulfur analog of Ebselen, has been reported to exhibit higher cytotoxicity than Ebselen itself [44], while other studies indicate that Ebsulfur and its derivatives, including N-alkyl compounds, exhibit lower hemolytic activity compared to Ebselen [45].

In this study, three derivatives of Ebsulfur (compounds **1**, **2**, and **3**, shown in Scheme 1), were tested against SPU and *Canavalia ensiformis* (jack bean) urease (JBU). Additionally, the selected derivatives allowed us to assess the influence of the alkyl substituent on the nitrogen atom, with compound **2** featuring a hydrophilic chain, compound **3** a hydrophobic chain, and compound **1** serving as the reference. Biochemical inhibition assays demonstrated that these Ebsulfur derivatives inactivate both bacterial and plant ureases in the low micromolar range. High-resolution X-ray structures on SPU co-crystallized in the presence of two of the tested compounds revealed the molecular basis for this reactivity. The mechanism involves a di-sulfuration event on the thiol group of αCys322, analogous to what was observed with Ebselen [25], leading to urease inactivation.

2. Materials and methods

2.1. Reagents and enzyme preparation

Compound **1** was purchased from ABCR (Karlsruhe, Germany) and used without further purification. Compounds **2** and **3** were synthesized and characterized (details in the Supplementary Material) according to procedures reported previously in the literature [46]. Urease from *Sporosarcina pasteurii* (SPU, molar mass: 250 kDa) was purified from the natural source [47–49] and stored at 4 °C at 11 mg mL^{-1} of active

protein in 50 mM HEPES buffer, 150 mM NaCl, 50 mM Na_2SO_3, and 2 mM EDTA, at pH 7.5. Urease from *Canavalia ensiformis* (jack bean) (JBU, molar mass: 550 kDa) type C-3 powder (≥ 600 units/μg) was purchased from Merck (Milan, Italy), dissolved to a concentration of 50 μg mL^{-1} of active protein in 20 mM HEPES buffer, at pH 7.5, and stored at −80 °C as stock aliquots. Quantification of both SPU and JBU was carried out using the pH-STAT method [50,51] by considering their specific activities (2.5 and 3.5 U μg^{-1} for SPU and JBU, respectively) [52].

2.2. IC_{50} measurements

100 mM stock solutions of compounds **1**, **2**, and **3** were prepared in pure DMSO and serially diluted in the same solvent to obtain 10-μL aliquots at concentrations ranging from 20 μM to 50 mM. Each aliquot was added with 990 μL of cresol red (CR) buffer (30 mg L^{-1} CR dissolved in 2 mM HEPES buffer, 2 mM EDTA, at pH 7.5), also containing 0.1–0.4 μg mL^{-1} of active SPU or JBU, resulting in enzyme incubation mixtures with compounds **1**, **2**, and **3** at concentrations ranging from 0.2 μM to 0.5 mM, and 10 % DMSO. After a one-hour incubation period, 987.5 μL of each incubation mixture was withdrawn and the enzymatic reaction was started by the addition of 12.5 μL of 8 M urea solution, resulting in a final urea concentration of 100 mM (ensuring saturating conditions for both SPU and JBU, which show Michaelis – Menten constants of *ca.* 17 mM and 4 mM, respectively [52]). The progress of the urease-catalyzed urea hydrolysis was monitored spectroscopically using an Agilent Cary 60 UV − Vis spectrophotometer, by following the overtime change in absorbance at 573 nm due to the change in colour of cresol red upon the increase of pH caused by urease activity. The initial reaction rate (v_i) was determined from the slope of the linear portion of the absorbance *vs.* time trace. Experiments were performed as triplicates, so averaged v_i values obtained at each concentration of the tested inhibitors were normalized to the averaged initial reaction rate determined in the absence of any inhibitor and in the presence of 10 % DMSO (v_0), and the resulting percentage enzyme residual activity values (experimental data available in Table 1-SI) were plotted as a function of inhibitor concentration on a semi-logarithmic graph. The IC_{50} values, representing the inhibitor concentration required to achieve 50 % enzyme inhibition, were estimated by fitting the data to the canonical dose-response curve using Prism v. 8.4.3 software.

2.3. Crystallization, data collection and structural determination

Aliquots of 11 mg mL^{-1} SPU were buffer-exchanged through repeated cycles of dilution and concentration to remove Na_2SO_3 using 50 mM HEPES buffer, also containing 150 mM NaCl and 2 mM EDTA, at pH 7.5, and Amicon Ultra centrifugal filter units (MWCO 10 kDa, Merck). Stock solutions (50 mM) of compounds **1** and **2** were prepared in pure DMSO and added at a 1:10 (*v*/v) ratio to the buffer-exchanged 11 mg mL^{-1} aliquots of SPU, resulting in incubation mixtures containing 10 mg mL^{-1} SPU (equivalent to 40 μM $(\alpha\beta\gamma)_3$ heterotrimer) and 5 mM of each compound, in the presence of 10 % (v/v) DMSO. After approximately four hours of incubation, during which the enzyme activity was completely abolished (as confirmed by testing small amounts of the incubation mixtures in the presence of 100 mM urea into CR buffer), crystallization trials were set up by mixing 1.5 μL of the incubation mixtures with an equal volume of a precipitant consisting of 1.7–2.1 M $(NH_4)_2SO_4$ dissolved in 100 mM sodium citrate buffer, at pH 6.3. The resulting crystallization drops were equilibrated by vapor diffusion (hanging-drop method) at 293 K against 0.5 mL of the precipitant solution using EasyXtal 15-Well plates (Qiagen). Rice-grain shaped protein crystals (approximately 0.05 × 0.05 × 0.1 mm^3) grew after two weeks in the presence of 1.9–2.1 M $(NH_4)_2SO_4$. The crystals were harvested using LithoLoops cryoloops (Molecular Dimensions, Suffolk, U.K.) and transferred to a cryoprotectant solution consisting of 2.4 M $(NH_4)_2SO_4$ dissolved in 100 mM citrate buffer, 20% (*v*/v) ethylene glycol, also containing 2.5 mM of the testing compounds, at pH 6.3. The crystals were flash-cooled and stored in liquid nitrogen.

Diffraction data were collected at 100 K using synchrotron X-ray radiation at the EMBL P13 beamline of the Petra III storage ring, DESY, Hamburg, Germany [53]. The diffraction data were processed and reduced using XDS [54] and AIMLESS [55,56]. The X-ray crystal structure of SPU bound to catechol (PDB code: 5G4H, 1.50 Å resolution) [57], with solvent molecules and ligands removed, and after coordinates randomization by applying a 0.5 Å rigid-body translation using PDBSET [58], was used as the starting model to obtain the initial phases for the structure determination.

Restrained refinement was performed using REFMAC5 [59] and isotropic atomic displacement parameters (ADPs), including the hydrogen atoms in the riding positions. Manual model rebuilding, as well as water or ligand addition/inspection, was conducted using COOT [60,61]. Unbiased omit electron density maps for non-protein moieties were calculated using Fourier coefficients *Fo - Fc* and phases from the final cycle of restrained refinement before the incorporation of the ligands into the refining model.

The X-ray crystal structures of SPU bound to compounds **1** and **2** were determined at final resolutions of 1.95 and 1.96 Å, respectively. The corresponding structure factors and atomic coordinates were deposited in the Protein Data Bank with the accession codes 9REX and 9REY. Data collection and final refinement statistics for these two structures are provided in Table 2-SI. Per-residue Cα RMSD analysis of the reported structures was performed using the Match→Align tool in UCSF Chimera [27].

3. Results and discussion

To assess the efficacy of Ebsulfur-derivatives **1**, **2**, and **3** as urease inhibitors, dose-response studies were conducted on both SPU and JBU. The explored inhibitor concentrations varied between 0.2 μM and 0.5 mM following a one-hour incubation period. The resulting semi-log dose-response plots are presented in Fig. 2 (experimental data are also available in Table 1-SI). In all cases, the experimental data exhibit nearly sigmoidal profiles with Hill slopes in the range 1.8–2.1, ultimately reaching complete enzyme inactivation at inhibitor concentrations above 100 μM. The resulting IC_{50} values fall in the low micromolar range, with no significant differences observed between the two urease forms. These relatively low IC_{50} values confirm the efficient urease inactivation by these compounds, although not as efficient as Ebselen and its derivatives (the latter falling in the nM range) [24–26].

The analysis of the crystallographic structures determined using X-ray diffraction on crystals of SPU co-crystallized in the presence of compounds **1** and **2** revealed the typical $(\alpha\beta\gamma)_3$ quaternary structure of SPU. Comparison with the native enzyme (PDB code: 4CEU) also showed significant conservation in the backbone folding (average Cα RMSD values lower than 0.2 Å, see Table 3-SI). A *per*-residue RMSD analysis revealed that the largest Cα RMSD values are detectable in the mobile flap region, involving αCys322 and its nearby residues, namely αVal321, αHis323, and αHis324 (Fig. 3).

The overall structure was largely conserved compared to previously reported crystal structures of SPU inhibited by cysteine-directed ligands, such as β-mercaptoethanol (PDB code: 1UBP) [48], para-benzoquinone (PDB code: 5FSE) [49], hydroquinone (PDB code: 8A18) [62], catechol (PDB code: 5G4H) [57], thiram (PDB code: 8Q2E) [63], and an Ebselen derivative (PDB code: 7ZCY) [25]. The largest RMSD values were observed for αCys322, which directly undergoes modification, and for the neighboring residues αHis323 and αHis324, which experience local structural alterations due to increased steric hindrance. The overall active site architecture is also largely conserved (Table 4-SI and top rows in Fig. 4A,B).

The Ni(II) hydration environment in the active site, which in the native SPU state consists of i) a hydroxide ion (W(B)) bridging the two Ni (II) ions, ii) two well-ordered water molecules positioned near Ni(1) (W1) and Ni(2) (W2), and iii) a distal water molecule (W3) (as shown in

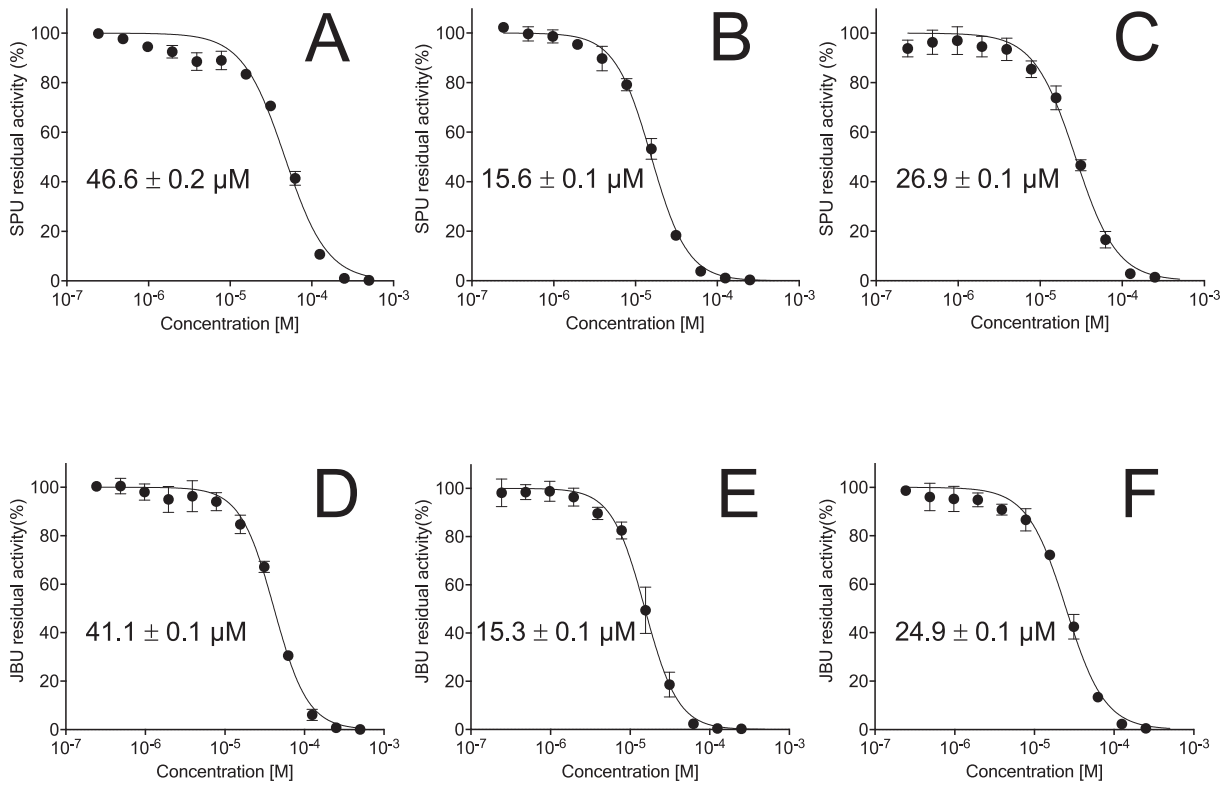

Fig. 2. Dose–response semi-log plots for the residual activity of SPU (panels A-C) and JBU (panels D—F) in the presence of increasing concentrations of compounds **1** (A or D), **2** (B or E), and **3** (C or F). Percentage enzyme residual activities (expressed as averaged values and relative error bars) and non-linear data fitting are shown as black dots and lines, respectively. IC_{50} values ± SD are also reported.

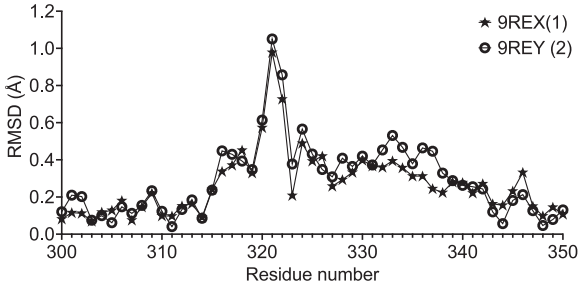

Fig. 3. Plot showing the *per-residue* Cα RMSD of the mobile flap region of the crystal structures of SPU *co*-crystallized in the presence of compounds **1** (PDB code: 9REX) and **2** (PDB code: 9REX) and bound to the di-nuclear S cluster calculated with respect to the crystal structure of native SPU (PDB code: 4CEU).

Fig. 1), remains fully conserved in the X-ray crystal structure of SPU co-crystallized with compound **1** (top panel in Fig. 4A). In contrast, for SPU co-crystallized with compound **2**, W1 and W2 are replaced by the OB1 and OB2 atoms of an anionic carboxylate group from a citrate moiety, which chelates the two Ni(II) ions in the active site (top panel in Fig. 4B). This interaction mirrors previous findings observed in the X-ray structure of SPU inhibited by citrate [64]. Citrate is a component of the SPU crystallization cocktail, and as suggested in the original paper, the presence of citrate bound to urease in the crystals likely results from partial drying during the hanging-drop crystallization process.

Following the refinement and model rebuilding of the protein structures, including the Ni(II) ions, solvent molecules, and other crystallization-derived ligands, unbiased omit electron density maps revealed additional positive regions near the solvent-exposed cysteine residues αCys322 and αCys555 of SPU. These regions, closely connected with the electron densities of the two cysteine Sγ atoms, strongly indicated the formation of covalent adducts at these residues.

The signals near αCys322 in the two structures exhibited a peculiar oblong shape (Fig. 1-SI), reminiscent of the electron density for two Se atoms as observed in the Ebselen-inactivated urease structure [25], suggesting the presence of two sulfur atoms. These were successfully modeled and refined with full occupancy (Fig. 4 bottom row): S(1) was refined bound to the Sγ atom of αCys322 at 2.1 Å, while S(2) was refined bound to S(1) at 2.1 Å (see Table 5-SI for distances and angles around the sulfur atoms). The di-sulfuration of αCys322 does not induce significant changes in the conformation of the mobile flap, which remains in the open state in both crystal structures. The local changes observed for the region around αCys322 (as shown by the per-residue Cα RMSD analysis presented in Fig. 3) only involve the residues directly affected by this covalent modification.

Additionally, the positive signals near αCys555 in both structures of SPU co-crystallized with **1** and **2** had composite shapes (Fig. 2-SI) suggesting the presence of each corresponding ligands bound to αCys555. Indeed, compounds **1** and **2** were successfully modeled and refined with full occupancy: the structures show the formation of a covalent bond between the sulfur atoms of **1** and **2** to the Sγ atom of αCys555 at 2.3 Å (Fig. 5).

The sulfur adducts observed through single-crystal X-ray diffraction of SPU treated with the two Ebsulfur derivatives **1** and **2** exhibit strong similarities to those found previously using an Ebselen derivative (PDB code: 7ZCY) [25]. This consistent evidence, combined with the similar properties of sulfur and selenium, strongly suggests a conserved reaction mechanism underlying the formation of the detected adducts (Fig. 6). The mechanistic hypothesis, initially proposed for Ebselen inhibition of the SARS-CoV-2 main protease [65], suggests the following steps (Fig. 6): (1) a nucleophilic attack by the thiolate form of the catalytic cysteine thiol (αCys322 in SPU), activated by the adjacent αHis323, on the sulfur atom of the ligand's five-membered ring, which opens the ring and forms an intermediate ligand bound through an S—S bond to the cysteine. This intermediate then undergoes an attack by a solvent

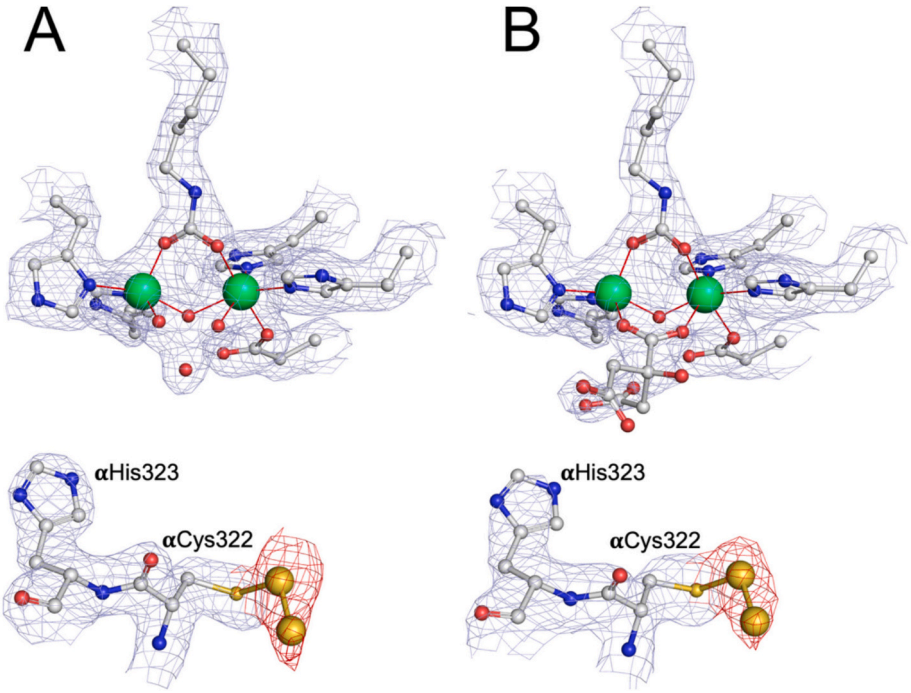

Fig. 4. Active site region of the X-ray crystal structure of SPU co-crystallized in the presence of compounds **1** (PDB code: 9REX) (A) and **2** (PDB code: 9REY) (B). The crystallographic model (carbon, nitrogen, oxygen, sulfur, and nickel atoms are colored grey, blue, red, yellow, and green, respectively) is shown superimposed to the final $2F_o - F_c$ electron density Fourier map, contoured at 1σ and colored light blue (top row). The two sulfur atoms bound to the thiol group of αCy322 residue upon enzyme inactivation by compounds **1** and **2** are shown superimposed to the final $2F_o - F_c$ map colored red (bottom row). Figures were generated using PyMol (The PyMOL Molecular Graphics System, v. 2.4.1, Schrödinger, LLC.). (For interpretation of the references to colour in this figure legend, the reader is referred to the web version of this article.)

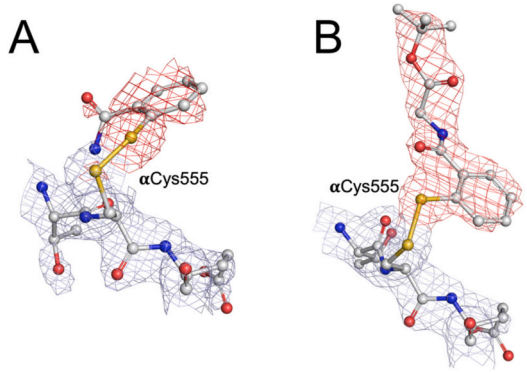

Fig. 5. Region proximal to the αCys555 residue of the X-ray crystal structure of SPU bound to compounds **1** (PDB code: 9REX) (A) and **2** (PDB code: 9REY) (B). The crystallographic model (carbon, nitrogen, oxygen, and sulfur atoms are colored grey, blue, red, and yellow, respectively) is shown superimposed to the final $2F_o - F_c$ electron density Fourier map, contoured at 1σ and colored light blue. The two ligands bound to the thiol group of αCy555 residue are shown superimposed to the final $2F_o - F_c$ map colored red. Figures were generated using PyMol (The PyMOL Molecular Graphics System, v. 2.4.1, Schrödinger, LLC.). (For interpretation of the references to colour in this figure legend, the reader is referred to the web version of this article.)

molecule activated by αHis323 (a process that apparently does not occur for αCys555 because of the absence of any nearby water-activating base), resulting in the hydrolysis of the C—S bond. The hydrolysis produces the final αCys322-Sγ-SH adduct. The presence of two sulfur atoms in the structures of SPU treated with the two Ebsulfur derivatives indicates that two consecutive reaction cycles occur at urease αCys322, leading to the di-sulfuration of its thiolate group and the formation of αCys322-Sγ-S-SH adduct. The adduct found at αCys555 corresponds to an intermediate of the same mechanism; however, the absence of a histidine residue adjacent to this site prevents the continuation of the reaction, highlighting the unique chemical environment of the active site mobile flap tip and providing strong support for the proposed reaction mechanism. The presence of two S atoms covalently bound to αCys322 in the reported X-ray crystal structures, together with the Hill slopes in the range 1.8–2.1 observed in the IC_{50} curves, is consistent with this mechanism.

According to the proposed reaction mechanism of urease [66], that involves (i) the closure of the flap upon the entrance of urea substrate in the active site cavity and (ii) the direct role of the αCys322 - αHis323 catalytic dyad in the proton transfer to the reaction intermediate during hydrolysis, the X-ray crystal structures of the adducts formed upon incubation of urease with compounds **1** and **2** provide strong evidence that the observed covalent modification of αCys322 alters either or both these processes. Moreover, the modification of αCys555 does not interfere with enzyme activity because this residue is located far away from the active site: the complete urease inactivation is fully driven by the modification occurring at the αCys322 site, as proven by the previously reported covalent modification of αCys322 by catechol [57] not involving Cys555, which resulted in full urease inactivation.

This mechanism helps the rationalization of the large difference in urease inactivation efficacy observed between Ebselen and Ebsulfur derivatives: the larger polarizability of Se as compared to S [67], together with the lower Se—C and Se—N bond dissociation energies compared to their corresponding S—C and S—N bonds [68], render the Ebselen derivatives more prone to react with the thiol moiety of cysteine residues, leading to the facilitated formation of a Cys-Sγ-Se bond and to the ring opening step, followed, in the case of αCys322, to the eventual formation of the Cys-Sγ-Se-Se-H covalent adduct, causing total loss of urease activity.

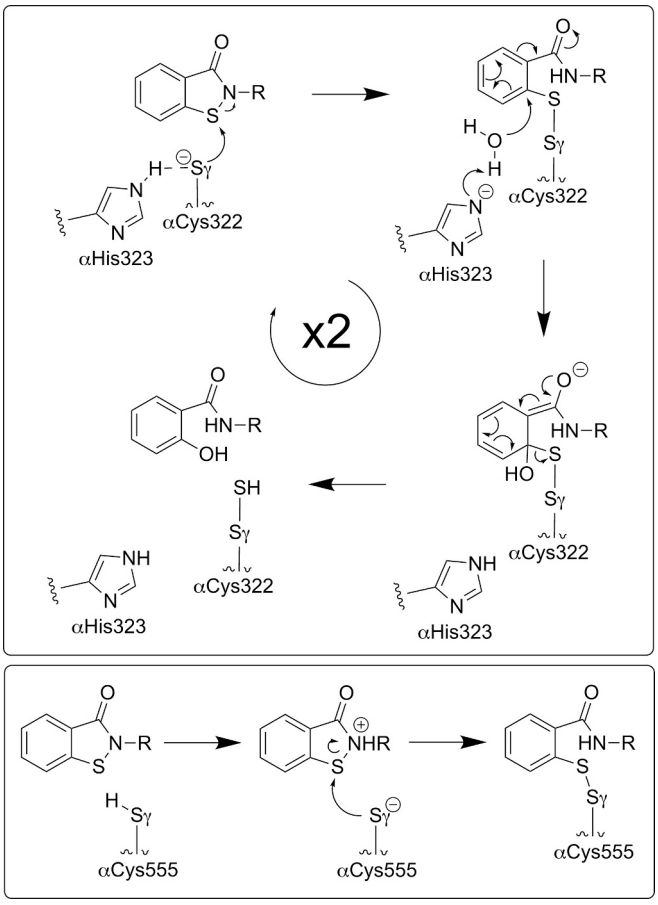

Fig. 6. Proposed reaction mechanism to rationalize the covalent modifications of αCys322 and αCys555 revealed in the crystal structures of *Sporosarcina pasteurii* urease inactivated by **1** and **2** (R = H or the moieties in compounds **1**–**3**).

4. Conclusions

The rise of antimicrobial resistance demands innovative therapeutic strategies, particularly against bacterial pathogens relying on urease activity for survival and virulence. Our study demonstrates that Ebsulfur derivatives effectively inhibit bacterial ureases, providing a mechanistic foundation for their potential development as antimicrobial agents. Structural insights confirm that these compounds target the catalytic cysteine residue, leading to enzyme inactivation via di-sulfuration. Compared to Ebselen, Ebsulfur derivatives exhibit a lower efficacy, but their potentially improved toxicological profile renders them attractive candidates for further pharmacological exploration and for the development of novel urease-targeting therapies.

This study is focused on an integrated biochemical and structural investigation aimed at determining the molecular details of the inhibition mechanism of a new class of potential urease-targeting drugs and should be considered prodromic to more biological and cellular investigations. The tested compounds, although representing a limited set, can be considered a first step towards a more comprehensive SAR study.

CRediT authorship contribution statement

Luca Mazzei: Writing – review & editing, Writing – original draft, Investigation, Data curation, Conceptualization. **Arundhati Paul:** Writing – review & editing, Investigation. **Michele Cianci:** Writing – review & editing, Methodology, Data curation. **Andrea Pizzi:** Writing – review & editing, Resources. **Giuseppe Resnati:** Writing – review & editing, Resources, Conceptualization. **Stefano Ciurli:** Writing – review & editing, Writing – original draft, Supervision, Funding acquisition, Conceptualization.

Declaration of competing interest

The authors declare that they have no known competing financial interests or personal relationships that could have appeared to influence the work reported in this paper.

Acknowledgments

This work was supported by the Consorzio Interuniversitario di Risonanze Magnetiche di Metallo-Proteine (CIRMMP), by the project "NICE – Nature Inspired Crystal Engineering" (PRIN2020), and by the University of Bologna.

Appendix A. Supplementary data

Supplementary data to this article can be found online at https://doi.org/10.1016/j.jinorgbio.2026.113272.

References

[1] C.J.L. Murray, K.S. Ikuta, F. Sharara, L. Swetschinski, G. Robles Aguilar, A. Gray, C. Han, C. Bisignano, P. Rao, E. Wool, et al. Global burden of bacterial antimicrobial resistance in 2019: a systematic analysis, Lancet (2022), 399 (10325), 629–655. doi:https://doi.org/10.1016/S0140-6736(21)02724-0.

[2] K.S. Ikuta, L.R. Swetschinski, G. Robles Aguilar, F. Sharara, T. Mestrovic, A.P. Gray, N. Davis Weaver, E.E. Wool, C. Han, A. Gershberg Hayoon, et al., Global mortality associated with 33 bacterial pathogens in 2019: a systematic analysis for the global burden of disease study 2019, Lancet 400 (10369) (2022) 2221–2248, https://doi.org/10.1016/S0140-6736(22)02185-7.

[3] I.N. Okeke, M.E.A. de Kraker, T.P. Van Boeckel, C.K. Kumar, H. Schmitt, A.C. Gales, S. Bertagnolio, M. Sharland, R. Laxminarayan, The scope of the antimicrobial resistance challenge, Lancet 403 (10442) (2024) 2426–2438, https://doi.org/10.1016/S0140-6736(24)00876-6.

[4] WHO, Prioritization of Pathogens to Guide Discovery, Research and Development of New Antibiotics for Drug-Resistant Bacterial Infections, Including Tuberculosis. https://www.who.int/publications/i/item/WHO-EMP-IAU-2017.12, 2017.

[5] WHO, WHO Bacterial Priority Pathogens List, 2024: Bacterial Pathogens of Public Health Importance to Guide Research, Development and Strategies to Prevent and Control Antimicrobial Resistance. https://www.who.int/publications/i/item/9789240093461, 2024.

[6] R.P. Hausinger, Nickel utilization by microorganisms, Microbiol. Rev. 51 (1987) 22–42, https://doi.org/10.1128/mr.51.1.22-42.1987.

[7] H.L. Mobley, R.P. Hausinger, Microbial ureases: significance, regulation, and molecular characterization, Microbiol. Rev. 53 (1989) 85–108, https://doi.org/10.1128/mr.53.1.85-108.1989.

[8] H.L. Mobley, M.D. Island, R.P. Hausinger, Molecular biology of microbial ureases, Microbiol. Rev. 59 (1995) 451–480, https://doi.org/10.1128/mr.59.3.451-480.1995.

[9] S. Ciurli, S. Benini, W.R. Rypniewski, K.S. Wilson, S. Miletti, S. Mangani, Structural properties of the nickel ions in urease: novel insights into the catalytic and inhibition mechanisms, Coord. Chem. Rev. 190-192 (1999) 331–355, https://doi.org/10.1016/S0010-8545(99)00093-4.

[10] B. Zambelli, F. Musiani, S. Benini, S. Ciurli, Chemistry of Ni^{2+} in urease: sensing, trafficking, and catalysis, Acc. Chem. Res. 44 (2011) 520–530, https://doi.org/10.1021/ar200041k.

[11] M.J. Maroney, S. Ciurli, Nonredox nickel enzymes, Chem. Rev. 114 (2014) 4206–4228, https://doi.org/10.1021/cr4004488.

[12] L. Mazzei, F. Musiani, S. Ciurli, Urease, in: D. Zamble, M. Rowińska-Żyrek, H. Kozlowski (Eds.), The Biological Chemistry of Nickel, Metallobiology Vol. 10, Royal Society of Chemistry, 2017, pp. 60–97, https://doi.org/10.1039/9781788010580.

[13] L. Mazzei, S. Ciurli, Urease, in: Encyclopedia of Inorganic and Bioinorganic Chemistry, John Wiley & Sons, Ltd, Chichester (UK), 2021, pp. 1–17, https://doi.org/10.1002/9781119951438.eibc2776.

[14] J.C. Rutherford, The emerging role of urease as a general microbial virulence factor, PLoS Pathog. 10 (2014) e1004062, https://doi.org/10.1371/journal.ppat.1004062.

[15] D. Mora, S. Arioli, Microbial urease in health and disease, PLoS Pathog. 10 (12) (2014) e1004472, https://doi.org/10.1371/journal.ppat.1004472.

[16] M.S. Algood Holly, L. Cover Timothy, *Helicobacter pylori* persistence: an overview of interactions between *H. pylori* and host immune defenses, Clin. Microbiol. Rev. 19 (4) (2006) 597–613, https://doi.org/10.1128/cmr.00006-06.

[17] Y.F. Rego, M.P. Queiroz, T.O. Brito, P.G. Carvalho, V.T. de Queiroz, A. de Fatima, F. Macedo Jr., A review on the development of urease inhibitors as antimicrobial agents against pathogenic bacteria, J. Adv. Res. 13 (2018) 69–100, https://doi.org/10.1016/j.jare.2018.05.003.

[18] D.M. Livermore, The need for new antibiotics, Clin. Microbiol. Infect. 10 (2004) 1–9, https://doi.org/10.1111/j.1465-0691.2004.1004.x.
[19] M. Miethke, M. Pieroni, T. Weber, M. Brönstrup, P. Hammann, L. Halby, P. B. Arimondo, P. Glaser, B. Aigle, H.B. Bode, et al., Towards the sustainable discovery and development of new antibiotics, Nat. Rev. Chem. 5 (10) (2021) 726–749, https://doi.org/10.1038/s41570-021-00313-1.
[20] Y. Liu, Z. Tong, J. Shi, R. Li, M. Upton, Z. Wang, Drug repurposing for next-generation combination therapies against multidrug-resistant bacteria, Theranostics 11 (10) (2021) 4910–4928, https://doi.org/10.7150/thno.56205.
[21] R. Nozawa, T. Yokota, T. Fujimoto, Susceptibility of methicillin-resistant *Staphylococcus aureus* to the selenium-containing compound 2-phenyl-1,2-benzoisoselenazol-3(2H)-one (PZ51), Antimicrob. Agents Chemother. 33 (8) (1989) 1388–1390, https://doi.org/10.1128/aac.33.8.1388.
[22] Y. Waleed, T. Shankar, N.S. Mohamed, Repurposing non-antimicrobial drugs and clinical molecules to treat bacterial infections, Curr. Pharm. Des. 21 (28) (2015) 4106–4111, https://doi.org/10.2174/1381612821666150506154434.
[23] E.J. Lenardão, C. Santi, L. Sancineto, Bioactive organoselenium compounds and therapeutic perspectives, in: New Frontiers in Organoselenium Compounds, Springer Cham, 2018, pp. 99–143, https://doi.org/10.1007/978-3-319-92405-2_2.
[24] K. Macegoniuk, E. Grela, J. Palus, E. Rudzińska-Szostak, A. Grabowiecka, M. Biernat, Ł. Berlicki, 1,2-Benzisoselenazol-3(2H)-one derivatives as a new class of bacterial urease inhibitors, J. Med. Chem. 59 (17) (2016) 8125–8133, https://doi.org/10.1021/acs.jmedchem.6b00986.
[25] K. Macegoniuk, W. Tabor, L. Mazzei, M. Cianci, M. Giurg, K. Olech, M. Burda-Grabowska, R. Kaleta, A. Grabowiecka, A. Mucha, et al., Optimized Ebselen-based inhibitors of bacterial ureases with nontypical mode of action, J. Med. Chem. 66 (3) (2023) 2054–2063, https://doi.org/10.1021/acs.jmedchem.2c01799.
[26] M. Grabarek, W. Tabor, P. Krzyżek, A. Grabowiecka, Ł. Berlicki, A. Mucha, Halogenated N-Benzylbenzisoselenazolones efficiently inhibit *Helicobacter pylori* ureolysis in vitro, ACS Med. Chem. Lett. 16 (4) (2025) 675–680, https://doi.org/10.1021/acsmedchemlett.5c00057.
[27] E.F. Pettersen, T.D. Goddard, C.C. Huang, G.S. Couch, D.M. Greenblatt, E.C. Meng, T.E. Ferrin, UCSF chimera - a visualization system for exploratory research and analysis, J. Comput. Chem. 25 (2004) 1605–1612, https://doi.org/10.1002/jcc.20084.
[28] C.W. Nogueira, N.V. Barbosa, J.B.T. Rocha, Toxicology and pharmacology of synthetic organoselenium compounds: an update, Arch. Toxicol. 95 (4) (2021) 1179–1226, https://doi.org/10.1007/s00204-021-03003-5.
[29] M.J. Parnham, H. Sies, The early research and development of ebselen, Biochem. Pharmacol. 86 (9) (2013) 1248–1253, https://doi.org/10.1016/j.bcp.2013.08.028.
[30] G.K. Azad, R.S. Tomar, Ebselen, a promising antioxidant drug: mechanisms of action and targets of biological pathways, Mol. Biol. Rep. 41 (8) (2014) 4865–4879, https://doi.org/10.1007/s11033-014-3417-x.
[31] C.W. Nogueira, G. Zeni, J.B.T. Rocha, Organoselenium and organotellurium compounds: toxicology and pharmacology, Chem. Rev. 104 (12) (2004) 6255–6286, https://doi.org/10.1021/cr0406559.
[32] C.W. Nogueira, J.B.T. Rocha, Toxicology and pharmacology of selenium: emphasis on synthetic organoselenium compounds, Arch. Toxicol. 85 (11) (2011) 1313–1359, https://doi.org/10.1007/s00204-011-0720-3.
[33] D. Morin, R. Zini, H. Ligeret, W. Neckameyer, S. Labidalle, J.-P. Tillement, Dual effect of ebselen on mitochondrial permeability transition, Biochem. Pharmacol. 65 (10) (2003) 1643–1651, https://doi.org/10.1016/S0006-2952(03)00114-X.
[34] V. Gogvadze, S.D. Klein, M. Shigenaga, B.N. Ames, C. Richter, Effect of ebselen on Ca2+ transport in mitochondria, Redox Rep. 5 (6) (2000) 359–363, https://doi.org/10.1179/135100000101535924.
[35] C.F. Yang, H.M. Shen, C.N. Ong, Intracellular thiol depletion causes mitochondrial permeability transition in ebselen-induced apoptosis, Arch. Biochem. Biophys. 380 (2) (2000) 319–330, https://doi.org/10.1006/abbi.2000.1939.
[36] S.T. Miorelli, R.M. Rosa, D.J. Moura, J.C. Rocha, L.A. Lobo, J.A. Henriques, J. Saffi, Antioxidant and anti-mutagenic effects of ebselen in yeast and in cultured mammalian V79 cells, Mutagenesis 23 (2) (2008) 93–99, https://doi.org/10.1093/mutage/gem048.
[37] G.K. Azad, S.J. Balkrishna, N. Sathish, S. Kumar, R.S. Tomar, Multifunctional Ebselen drug functions through the activation of DNA damage response and alterations in nuclear proteins, Biochem. Pharmacol. 83 (2) (2012) 296–303, https://doi.org/10.1016/j.bcp.2011.10.011.
[38] J.L. Larabee, J.R. Hocker, J.S. Hanas, Mechanisms of inhibition of zinc-finger transcription factors by selenium compounds ebselen and selenite, J. Inorg. Biochem. 103 (3) (2009) 419–426, https://doi.org/10.1016/j.jinorgbio.2008.12.007.
[39] C.-F. Yang, H.-M. Shen, C.-N. Ong, Ebselen induces apoptosis in HepG2 cells through rapid depletion of intracellular thiols, Arch. Biochem. Biophys. 374 (2) (2000) 142–152, https://doi.org/10.1006/abbi.1999.1574.
[40] K.H. Lee, D. Jeong, Bimodal actions of selenium essential for antioxidant and toxic pro-oxidant activities: the selenium paradox (review), Mol. Med. Rep. 5 (2) (2012) 299–304, https://doi.org/10.3892/mmr.2011.651.
[41] A. Razaghi, M. Poorebrahim, D. Sarhan, M. Björnstedt, Selenium stimulates the antitumour immunity: insights to future research, Eur. J. Cancer 155 (2021) 256–267, https://doi.org/10.1016/j.ejca.2021.07.013.
[42] E. Uysal, B. Yaman, Selenium: the cancer shield, J. Biosci. Med. 12 (7) (2024) 170–183, https://doi.org/10.4236/jbm.2024.127016.
[43] D. Nair, E. Rådestad, P. Khalkar, N. Diaz-Argelich, A. Schröder, C. Klynning, J. Ungerstedt, M. Uhlin, A.P. Fernandes, Methylseleninic acid sensitizes ovarian cancer cells to T-cell mediated killing by decreasing PDL1 and VEGF levels, Front. Oncol. 8 (2018) 407, https://doi.org/10.3389/fonc.2018.00407.
[44] M.J. Parnham, J. Biedermann, C. Bittner, N. Dereu, S. Leyck, H. Wetzig, Structure-activity relationships of a series of anti-inflammatory benzisoselenazolones (BISAs), Agents Actions 27 (3) (1989) 306–308, https://doi.org/10.1007/BF01972806.
[45] H.X. Ngo, S.K. Shrestha, K.D. Green, S. Garneau-Tsodikova, Development of ebsulfur analogues as potent antibacterials against methicillin-resistant *Staphylococcus aureus*, Bioorg. Med. Chem. 24 (24) (2016) 6298–6306, https://doi.org/10.1016/j.bmc.2016.03.060.
[46] F. Viani, B. Rossi, W. Panzeri, L. Merlini, A.M. Martorana, A. Polissi, Y.M. Galante, Synthesis and anti-bacterial activity of a library of 1,2-benzisothiazol-3(2H)-one (BIT) derivatives amenable of crosslinking to polysaccharides, Tetrahedron 73 (13) (2017) 1745–1761, https://doi.org/10.1016/j.tet.2017.02.025.
[47] L. Mazzei, M. Cianci, S. Benini, L. Bertini, F. Musiani, S. Ciurli, Kinetic and structural studies reveal a unique binding mode of sulfite to the nickel center in urease, J. Inorg. Biochem. 154 (2016) 42–49, https://doi.org/10.1016/j.jinorgbio.2015.11.003.
[48] S. Benini, W.R. Rypniewski, K.S. Wilson, S. Ciurli, S. Mangani, The complex of *Bacillus pasteurii* urease with b-mercaptoethanol from X-ray data at 1.65 Å resolution, J. Biol. Inorg. Chem. 3 (4) (1998) 268–273, https://doi.org/10.1007/s007750050231.
[49] L. Mazzei, M. Cianci, F. Musiani, S. Ciurli, Inactivation of urease by 1,4-benzoquinone: chemistry at the protein surface, Dalton Trans. 45 (13) (2016) 5455–5459, https://doi.org/10.1039/c6dt00652c.
[50] R.L. Blakeley, E.C. Webb, B. Zerner, Jack bean urease (EC 3.5.1.5). A new purification and reliable rate assay, Biochemistry 8 (5) (1969) 1984–1990, https://doi.org/10.1021/bi00833a031.
[51] S. Benini, C. Gessa, S. Ciurli, *Bacillus pasteurii* urease: a heteropolymeric enzyme with a binuclear nickel active site, Soil Biol. Biochem. 28 (6) (1996) 819–821, https://doi.org/10.1016/0038-0717(96)00017-X.
[52] B. Krajewska, Ureases I. Functional, catalytic and kinetic properties: a review, J. Mol. Catal. B Enzym. 59 (1–3) (2009) 9–21, https://doi.org/10.1016/j.molcatb.2009.01.003.
[53] M. Cianci, G. Bourenkov, G. Pompidor, I. Karpics, J. Kallio, I. Bento, M. Roessle, F. Cipriani, S. Fiedler, T.R. Schneider, P13, the EMBL macromolecular crystallography beamline at the low-emittance PETRA III ring for high- and low-energy phasing with variable beam focusing, J. Synchrotron Radiat. 24 (1) (2017) 323–332, https://doi.org/10.1107/S1600577516016465.
[54] W. Kabsch, Xds, Acta Crystallogr. D Biol. Crystallogr. 66 (Pt 2) (2010) 125–132, https://doi.org/10.1107/S0907444909047337.
[55] P.R. Evans, Scaling and assessment of data quality, Acta Crystallogr. D Biol. Crystallogr. 62 (Pt 1) (2006) 72–82, https://doi.org/10.1107/S0907444905036693.
[56] P.R. Evans, An introduction to data reduction: space-group determination, scaling and intensity statistics, Acta Crystallogr. D Biol. Crystallogr. 67 (Pt 4) (2011) 282–292, https://doi.org/10.1107/S090744491003982X.
[57] L. Mazzei, M. Cianci, F. Musiani, G. Lente, M. Palombo, S. Ciurli, Inactivation of urease by catechol: kinetics and structure, J. Inorg. Biochem. 166 (2017) 182–189, https://doi.org/10.1016/j.jinorgbio.2016.11.016.
[58] Collaborative Computational Project Number 4, The CCP4 suite: programs for protein crystallography, Acta Crystallogr. D Biol. Crystallogr. 50 (Pt 5) (1994) 760–763, https://doi.org/10.1107/S0907444994003112.
[59] G.N. Murshudov, A.A. Vagin, E.J. Dodson, Refinement of macromolecular structures by the maximum-likelihood method, Acta Crystallogr. D Biol. Crystallogr. 53 (Pt 3) (1997) 240–255, https://doi.org/10.1107/S0907444996012255.
[60] P. Emsley, B. Lohkamp, W.G. Scott, K. Cowtan, Features and development of coot, Acta Crystallogr. D Biol. Crystallogr. 66 (Pt 4) (2010) 486–501, https://doi.org/10.1107/S0907444910007493.
[61] P. Emsley, K. Cowtan, Coot: model-building tools for molecular graphics, Acta Crystallogr. D Biol. Crystallogr. 60 (Pt 12) (2004) 2126–2132, https://doi.org/10.1107/S0907444904019158.
[62] L. Mazzei, M. Cianci, S. Ciurli, Inhibition of urease by hydroquinones: a structural and kinetic study, Chem. Eur. J. 28 (64) (2022) e202201770, https://doi.org/10.1002/chem.202201770.
[63] L. Mazzei, A. Paul, M. Cianci, M. Devodier, D. Mandelli, P. Carloni, S. Ciurli, Kinetic and structural details of urease inactivation by thiuram disulphides, J. Inorg. Biochem. 250 (2024) 112398, https://doi.org/10.1016/j.jinorgbio.2023.112398.
[64] S. Benini, P. Kosikowska, M. Cianci, L. Mazzei, A.G. Vara, L. Berlicki, S. Ciurli, The crystal structure of *Sporosarcina pasteurii* urease in a complex with citrate provides new hints for inhibitor design, J. Biol. Inorg. Chem. 18 (3) (2013) 391–399, https://doi.org/10.1007/s00775-013-0983-7.
[65] K. Amporndanai, X. Meng, W. Shang, Z. Jin, M. Rogers, Y. Zhao, Z. Rao, Z.-J. Liu, H. Yang, L. Zhang, et al., Inhibition mechanism of SARS-CoV-2 main protease by ebselen and its derivatives, Nat. Commun. 12 (1) (2021) 3061, https://doi.org/10.1038/s41467-021-23313-7.
[66] L. Mazzei, M. Cianci, S. Benini, S. Ciurli, The structure of the elusive urease-urea complex unveils the mechanism of a paradigmatic nickel-dependent enzyme, Angew Chem Int, Engl 58 (22) (2019) 7415–7419, https://doi.org/10.1002/anie.201903565.
[67] L.A. Wessjohann, A. Schneider, M. Abbas, W. Brandt, Selenium in chemistry and biochemistry in comparison to sulfur, Biol. Chem. 388 (10) (2007) 997–1006, https://doi.org/10.1515/BC.2007.138.
[68] W.M. Haynes (Ed.), Handbook of Chemistry and Physics, CRC Press, Boca Raton, USA, 2016.